

Supporting Information

Double boron atoms doped Graphdiyne as efficient metal-free electrocatalysts for nitrogen reduction into ammonia: A First-Principles Study

Cheng Fu, Yafei Li* and Haiyan Wei*

**Jiangsu Key Laboratory of Biofunctional Materials, School of Chemistry and Materials Science, Jiangsu Key Lab for NSLSCS, Nanjing Normal University, Nanjing 210097, China. E-mail: liyafei@njnu.edu.cn, weihaiyan@njnu.edu.cn*

Electronic Supplementary Information (ESI) available: [details of any supplementary information available should be included here]. See DOI: 10.1039/x0xx00000x

- 1. Table S1.** The cohesive energies of pristine-GDY and double boron atoms doped GDY-2B configurations.
- 2. Scheme. S1.** Schematic depiction of the distal pathway and alternating pathway for NRR on configuration GDY-2B via end-on N₂ adsorption mode.
- 3. Fig. S1.** Optimized structures (top-view and side-view) for (a) pristine-GDY, (b) GDY-2B(S₁S₁'), (c) GDY-2B(S₂S₂'), (d) GDY-2B(S₂S₃'), (e) GDY-2B(S₃S₃'), (f) GDY-2B(A₁A₁'), (g) GDY-2B(A₁A₂), (h) GDY-2B(A₁A₃), (i) GDY-2B(S₁A₁), (j) GDY-2B(S₂A₁), (k) GDY-2B(S₃A₁), (l) GDY-2B(S₄A₁). Brown and pink balls stand for carbon and boron atoms respectively.
- 4. Fig. S2.** Optimized structures with bond length (Å) labeled for (a) GDY-2B(S₁S₁'), (b) GDY-2B(S₂S₂'), (c) GDY-2B(S₂S₃'), (d) GDY-2B(A₁A₁'), (e) GDY-2B(A₁A₂), (f) GDY-2B(S₄A₁).
- 5. Fig. S3.** The Bader charge values on (a) pristine-GDY and GDY-2B configurations (b) GDY-2B(S₁S₁'), (c) GDY-2B(S₂S₂'), (d) GDY-2B(S₂S₃'), (e) GDY-2B(A₁A₁'), (f) GDY-2B(A₁A₂), (g) GDY-2B(S₄A₁).
- 6. Fig. S4.** Total density of states (TDOS) and partial density of states (PDOS) of (a) GDY-2B(S₁S₁'), (b) GDY-2B(S₂S₂'), (c) GDY-2B(S₂S₃'), (d) GDY-2B(A₁A₁'), (e) GDY-2B(A₁A₂) and (f) GDY-2B(S₄A₁). The Fermi level is set to zero, as shown by the black dashed line.
- 7. Fig. S5.** Potential energy surfaces for NRR on GDY-2B(S₄A₁) configuration through (a) consecutive, (b) enzymatic mechanisms as the hydrogenation beginning at the S₄-site B atom at different applied potentials, together with free energy and (c) the relative geometric structures for each elementary step.
- 8. Fig. S6.** Potential energy surfaces for NRR on GDY-2B(A₁A₁') configuration through (a) consecutive, (b) enzymatic, (c) distal and (d) alternating mechanisms at different applied potentials, together with free energy and the relative geometric structures for each elementary step of (e) consecutive and enzymatic mechanisms, and (f) distal and alternating mechanisms.
- 9. Fig. S7.** Potential energy surfaces for NRR on GDY-2B(A₁A₂) configuration through (a) consecutive, (b) enzymatic mechanisms as the hydrogenation beginning at the A₁-site B atom at different applied potentials, together with free energy and (c) the relative geometric structures for each elementary step.
- 10. Fig. S8.** Potential energy surfaces for NRR on GDY-2B(A₁A₂) configuration through (a) consecutive, (b) enzymatic mechanisms as the hydrogenation beginning at the A₂-site B atom at different applied potentials, together

with free energy and (c) the relative geometric structures for each elementary step.

11. Fig. S9. (a) Free energy diagram for the HER on GDY-2B(S₂S₂') and (b) the corresponding structures of GDY-2B(S₂S₂') with H atom adsorbed after optimization.

12. Fig. S10. The calculated band structure of (a) pristine-GDY and (b) GDY-2B(S₄A₁). The Fermi level is set to zero.

13. Fig. S11. The Bader charge values on N₂ adsorbed GDY-2B configurations via side-on mode on (a) GDY-2B(S₂S₂₁A₁'), (c) GDY-2B-(A₁A₂), (d) GDY-2B-(S₄A₁), and via end-on mode on (e) GDY-2B(A₁A₁'), respectively.

14. Fig. S12. (a) The electron density difference of N₂ molecule adsorbed on GDY-2B(S₄A₁) with the isosurface level set to be 0.002 e/Å³. Yellow and blue regions represent electron accumulation and depletion, respectively. (b) Partial density of states (PDOS) of N₂ molecule adsorbed on GDY-2B(S₄A₁) and the Fermi level is set to zero, as shown by the black dashed line.

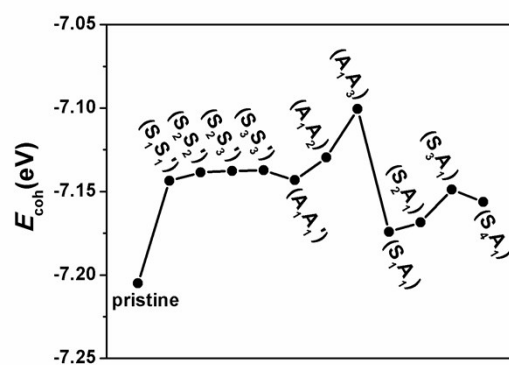
15. Fig. S13. (a) Definition of three moieties of N_xH_y adsorbed on GDY-2B(S₄A₁) by using *N-*NH as the model. (b) Charge variation of three moieties along the preferable enzymatic mechanism on GDY-2B(S₄A₁).

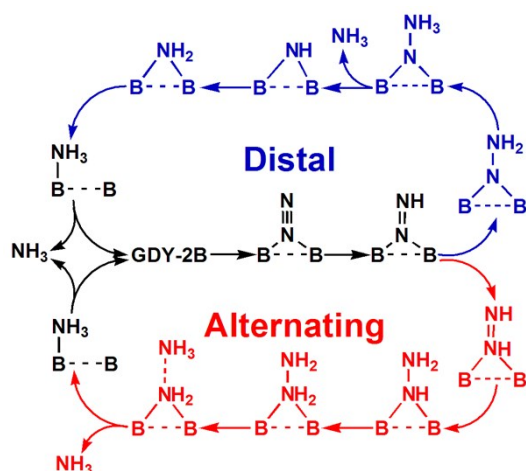
16. Fig. S14. Variations of temperature and energy against the time for AIMD simulations of GDY-2B(S₂S₂

17. Fig. S15. The corresponding structures of N₂ adsorption on pristine GDY (a) before and (b) after optimization in top-view and side-view.

Table S1. The cohesive energies of pristine-GDY and double boron atoms doped GDY-2B configurations.

Configuration	$E_{\text{coh}}(\text{eV})$
pristine-GDY	-7.205
GDY-2B(S ₁ S ₁ ')	-7.144
GDY-2B(S ₂ S ₂ ')	-7.139
GDY-2B(S ₂ S ₃ ')	-7.138
GDY-2B(S ₃ S ₃ ')	-7.137
GDY-2B(A ₁ A ₁ ')	-7.143
GDY-2B(A ₁ A ₂)	-7.130
GDY-2B(A ₁ A ₃)	-7.101
GDY-2B(S ₁ A ₁)	-7.174
GDY-2B(S ₂ A ₁)	-7.169
GDY-2B(S ₃ A ₁)	-7.149
GDY-2B(S ₄ A ₁)	-7.156





Scheme. S1. Schematic depiction of the distal pathway and alternating pathway for NRR on configuration GDY-2B via end-on N_2 adsorption mode.

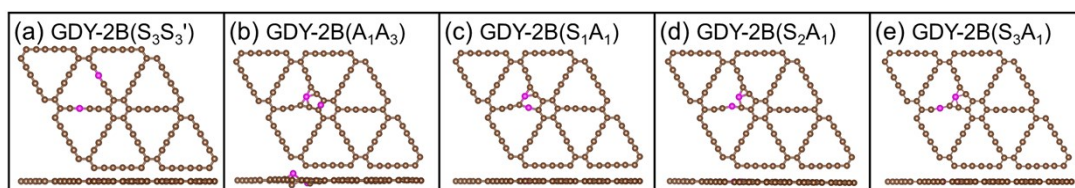


Fig. S1. Optimized structures (top-view and side-view) for (a) GDY-2B(S_3S_3'), (b) GDY-2B(A_1A_3), (c) GDY-2B(S_1A_1), (d) GDY-2B(S_2A_1), (e) GDY-2B(S_3A_1). Brown and pink balls stand for carbon and boron atoms respectively.

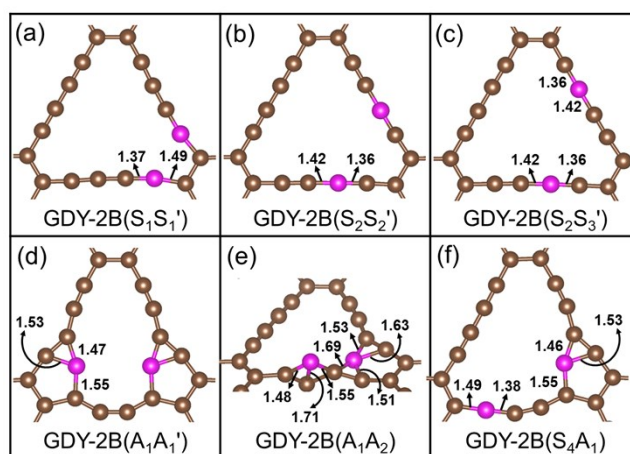


Fig. S2. Optimized structures with bond length (\AA) labeled for (a) GDY-2B(S_1S_1'), (b) GDY-2B(S_2S_2'), (c) GDY-2B(S_2S_3'), (d) GDY-2B(A_1A_1'), (e) GDY-2B(A_1A_2), (f) GDY-2B(S_4A_1).

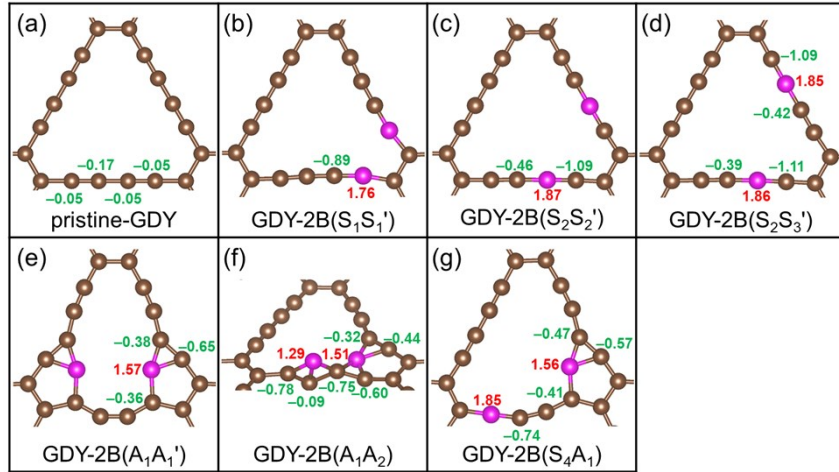


Fig. S3. The Bader charge values on (a) pristine-GDY and GDY-2B configurations (b) GDY-2B(S_1S_1'), (c) GDY-2B(S_2S_2'), (d) GDY-2B(S_2S_3'), (e) GDY-2B(A_1A_1'), (f) GDY-2B(A_1A_2), (g) GDY-2B(S_4A_1).

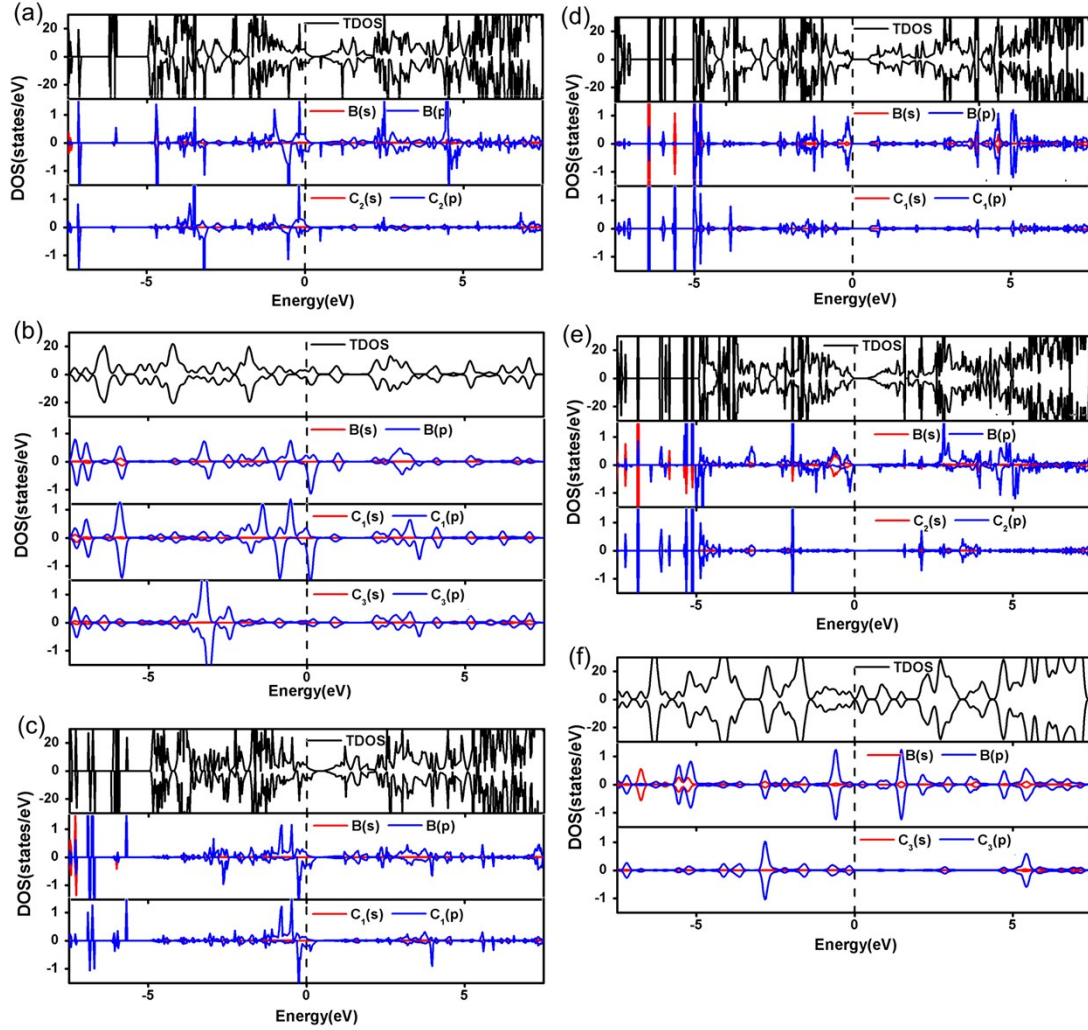


Fig. S4. Total density of states (TDOS) and partial density of states (PDOS) of (a) GDY-2B(S_1S_1'), (b) GDY-2B(S_2S_2'), (c) GDY-2B(S_2S_3'), (d) GDY-2B(A_1A_1'), (e) GDY-2B(A_1A_2) and (f) GDY-2B(S_4A_1). The Fermi level is set to zero, as shown by the black dashed line.

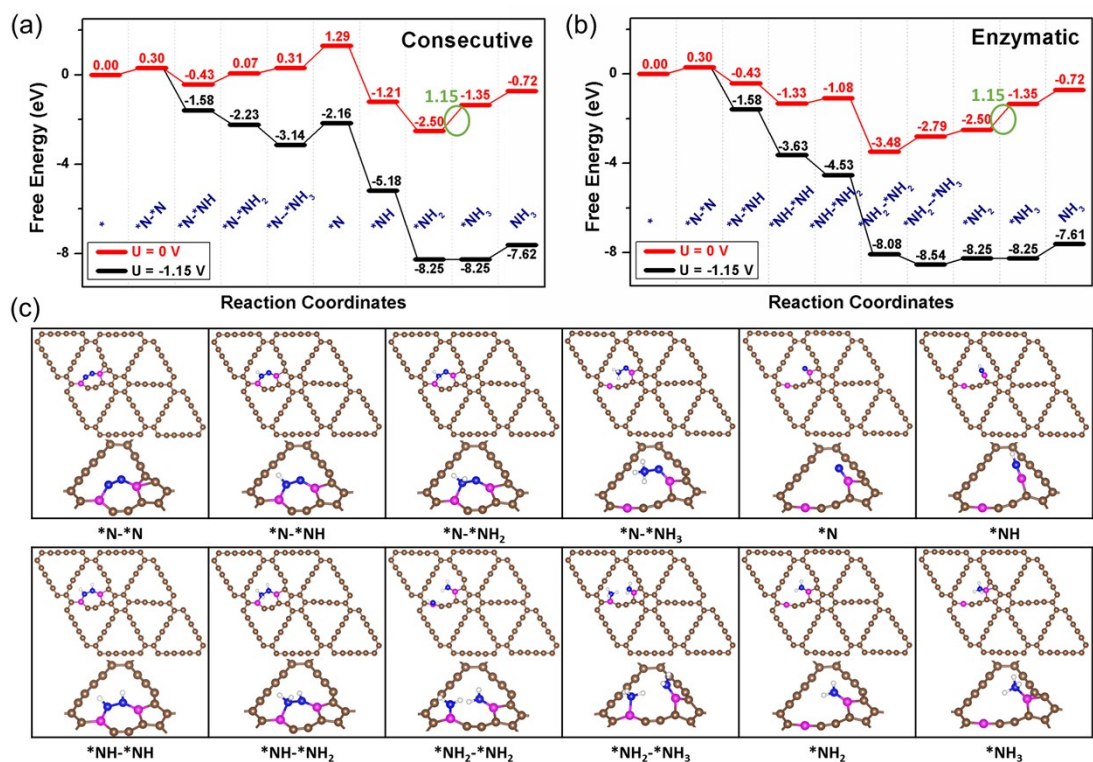


Fig. S5. Potential energy surfaces for NRR on GDY-2B(S₄A₁) configuration through (a) consecutive, (b) enzymatic mechanisms as the hydrogenation beginning at the S₄-site B atom at different applied potentials, together with free energy and (c) the relative geometric structures for each elementary step.

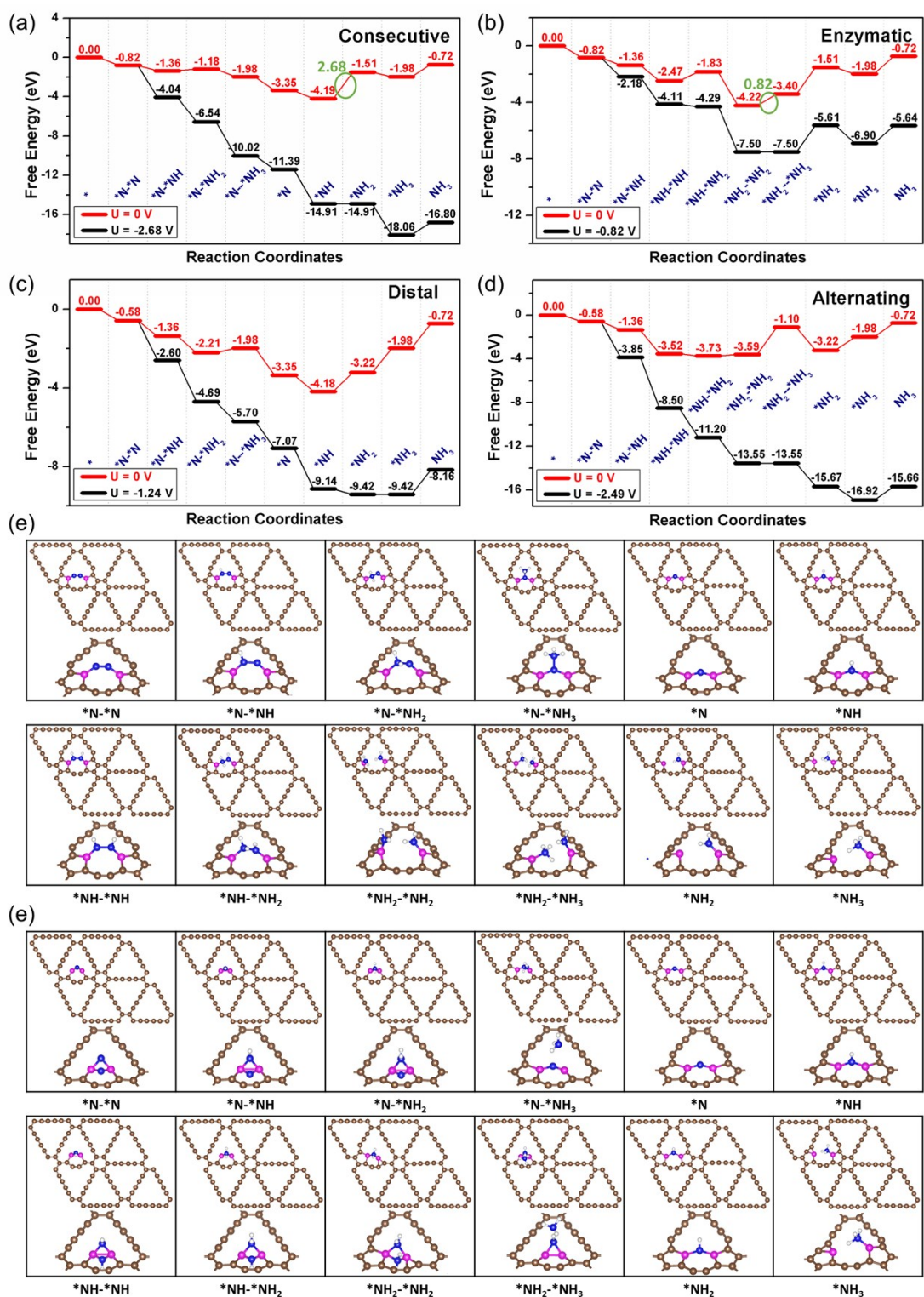


Fig. S6. Potential energy surfaces for NRR on GDY-2B(A₁A₁') configuration through (a) consecutive, (b) enzymatic, (c) distal and (d) alternating mechanisms at different applied potentials, together with free energy and the relative geometric structures for each elementary step of (e) consecutive and enzymatic mechanisms, and (f) distal and alternating mechanisms.

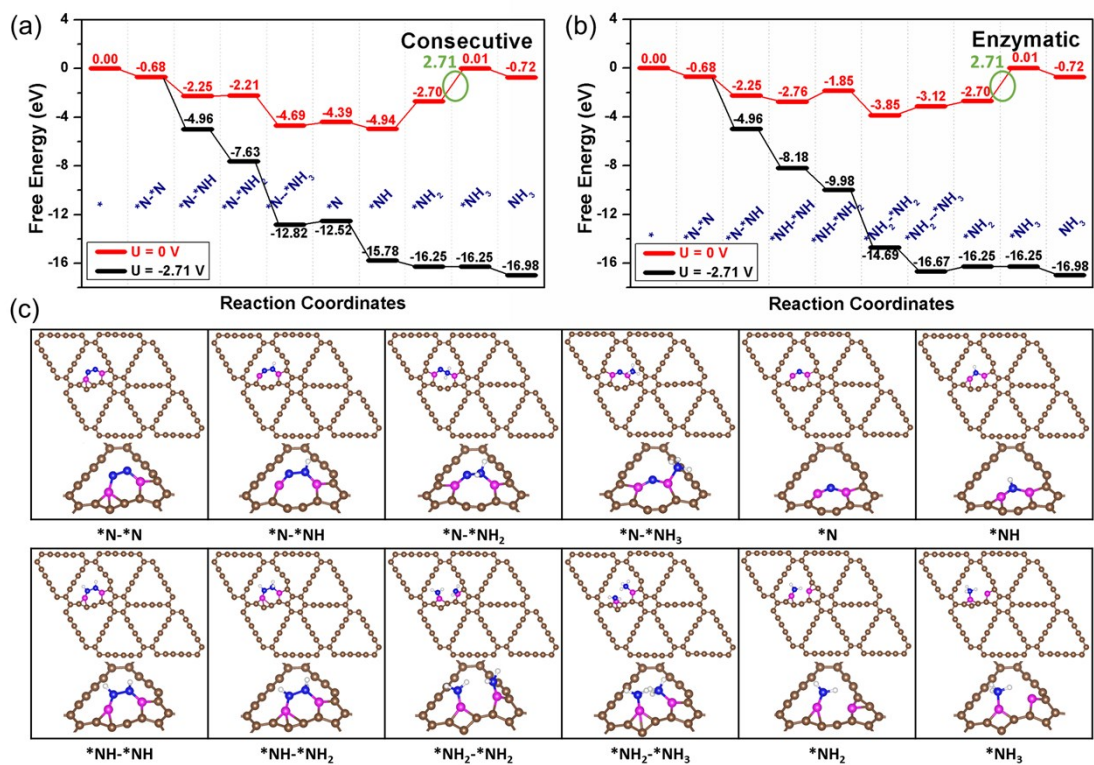


Fig. S7. Potential energy surfaces for NRR on GDY-2B(A₁A₂) configuration through (a) consecutive, (b) enzymatic mechanisms as the hydrogenation beginning at the A₁-site B atom at different applied potentials, together with free energy and (c) the relative geometric structures for each elementary step.

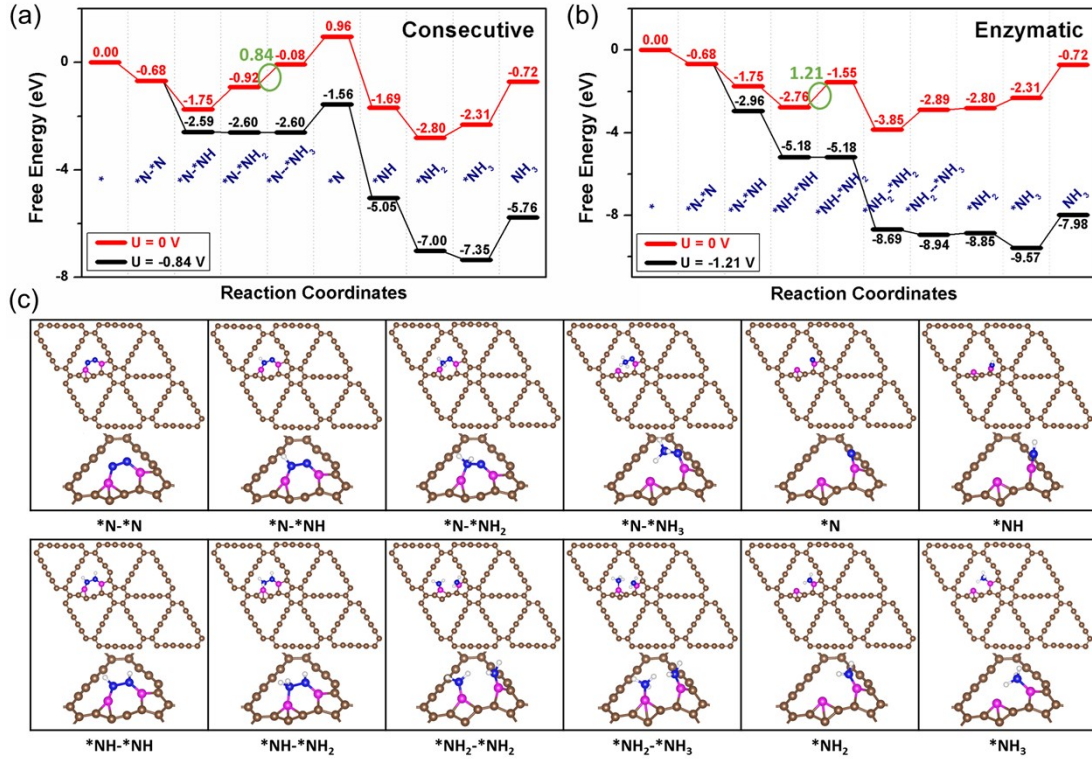


Fig. S8. Potential energy surfaces for NRR on GDY-2B(A₁A₂) configuration through (a) consecutive, (b) enzymatic mechanisms as the hydrogenation beginning at the A₂-site B atom at different applied potentials, together with free energy and (c) the relative geometric structures for each elementary step.

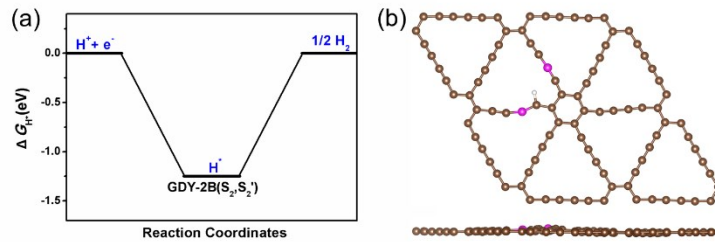


Fig. S9. (a) Free energy diagram for the HER on GDY-2B(S₂S₂') and (b) the corresponding structures of GDY-2B(S₂S₂') with H atom adsorbed after optimization.

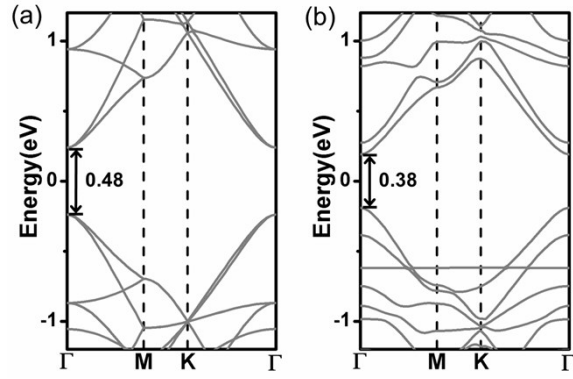


Fig. S10. The calculated band structure of (a) pristine-GDY and (b) GDY-2B(S_4A_1). The Fermi level is set to zero.

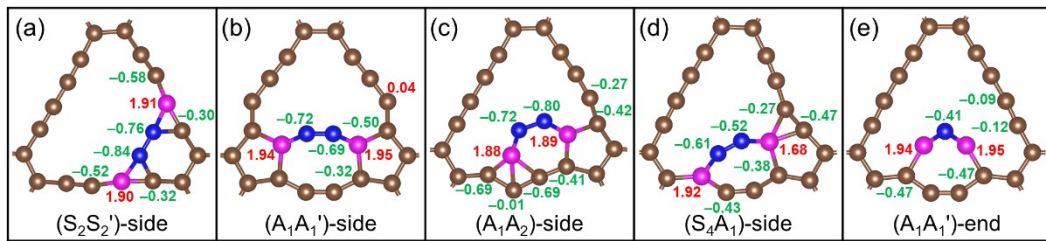


Fig. S11. The Bader charge values on N_2 adsorbed GDY-2B configurations via side-on mode on (a) GDY-2B(S_2S_2'), (b) GDY-2B(A_1A_1'), (c) GDY-2B(A_1A_2), (d) GDY-2B(S_4A_1), and via end-on mode on (e) GDY-2B(A_1A_1'), respectively.

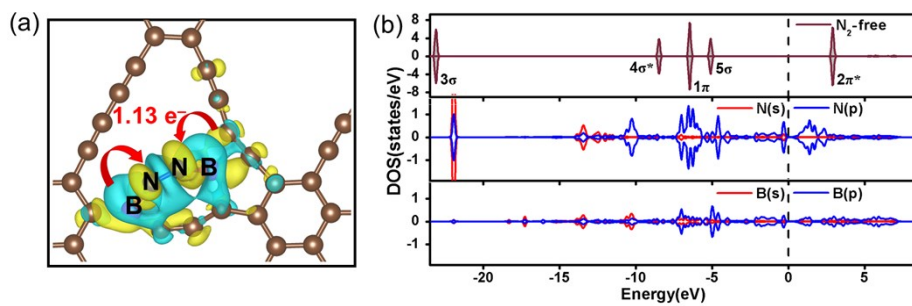


Fig. S12. (a) The electron density difference of N_2 molecule adsorbed on GDY-2B(S_4A_1) with the isosurface level set to be $0.002 \text{ e}/\text{\AA}^3$. Yellow and blue regions represent electron accumulation and depletion, respectively. (b) Partial density of states (PDOS) of N_2 molecule adsorbed on GDY-2B(S_4A_1) and the Fermi level is set to zero, as shown by the black dashed line.

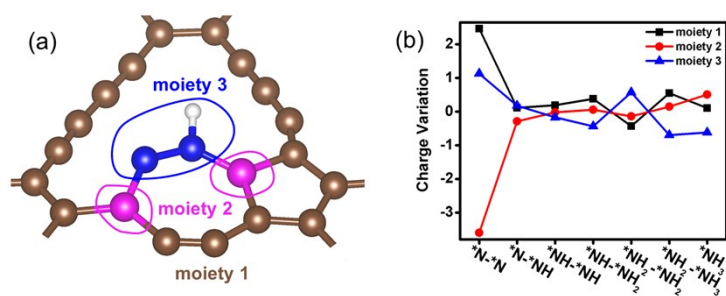


Fig. S13. (a) Definition of three moieties of N_xH_y adsorbed on GDY-2B(S₄A₁) by using *N-*NH as the model. (b) Charge variation of three moieties along the preferable enzymatic mechanism on GDY-2B(S₄A₁).

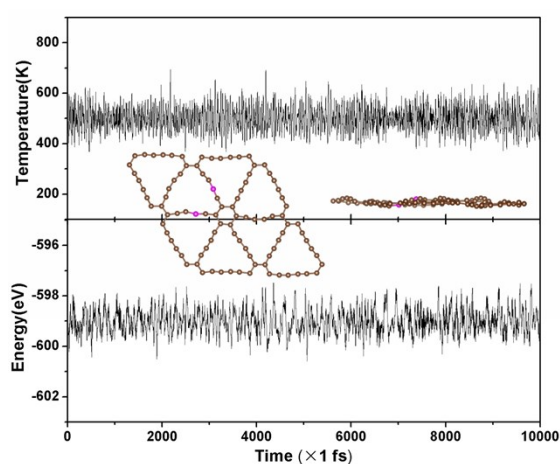


Fig. S14. Variations of temperature and energy against the time for AIMD simulations of GDY-2B(S₂S₂'), and inserts are top and side views of the snapshot of the atomic configuration. The simulation is run under 500 K for 10 ps with a time step of 1 fs.

Ab initio molecular dynamics (AIMD) simulations are performed in the canonical ensemble (NVT), with the temperature controlled by the Nosé–Hoover thermostat approach (J. Chem. Phys. 1984, 81, 511–518/ Phys. Rev. A 1985, 31, 1695–1697). And the simulations are run for a time period of 10.0 ps with a typical time interval of 1 fs under 500 K.

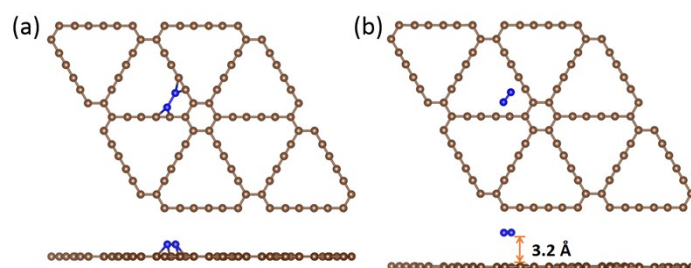


Fig. S15. The corresponding structures of N₂ adsorption on pristine GDY (a) before and (b) after optimization in top-view and side-view.